# Future population-adjusted heat stress extremes over the Great Lakes Region

TC Chakraborty[1*], Jiali Wang[2], Zhao Yang[1], Yun Qian[1], William Pringle[2], and Pengfei Xue[2,3]

[1] Atmospheric Sciences and Global Change Division, Pacific Northwest National Laboratory, Richland, WA 99352, USA

[2] Environmental Science Division, Argonne National Laboratory, 9700 South Cass Avenue, Lemont, IL 60439, USA

[3] Department of Civil, Environmental and Geospatial Engineering, Michigan Technological University, Houghton, MI 49931, USA

*Corresponding author: tc.chakraborty@pnnl.gov

**Key Points:**

- Pseudo global warming simulations used to dynamically downscale future climate projections over Great Lakes Region.
- Future population growth can more than double population-adjusted heat stress above high heat stress thresholds.
- Humidity change in the future amplified outdoor moist heat stress exposure in the region across models.

**Abstract**

There are large uncertainties in our future projections of climate change at the regional scale, with spatial variabilities not resolved adequately by coarse-grained Earth System Models (ESMs). In this study, we use pseudo global warming simulations driven by end of the century upper end RCP (Representative Concentration Pathway) 8.5 projections from 11 state-of-the-art ESMs to examine changes in summer heat stress extremes using physiologically relevant heat stress metrics (heat index and wet bulb globe temperature) over the Great Lakes Region (GLR). These simulations, generated from a cloud-resolving model, are at a fine spatiotemporal resolution to detect heterogeneities relevant for human heat exposure. These downscaled climate projections are combined with gridded future population estimates to isolate population versus warming contributions to population-adjusted heat stress in this region. Our results show that a significant portion of summer will be dominated by critical outdoor heat stress levels within GLR for this scenario. Additionally, regions with higher heat stress generally have disproportionately higher population densities. Humidity change generates positive feedback on future heat stress, generally amplifying heat stress (by 24.2% to 79.5%) compared to changing air temperature alone, with the degree of control of humidity depending on the heat stress metric used. The uncertainty of the results for future heat stress are quantified based on multiple ESMs and heat stress metrics used in this study. Overall, our study shows the importance of dynamically resolving heat stress at population-relevant scales to get more accurate estimates of future heat risk in the region.

**Plan Language Summary**

Global models used to predict future climate usually run over grids that are too large to examine regional variations. So, here we use a numerical model driven by several global models to predict future changes over the Great Lakes Region for smaller grids. These predictions are then combined with predictions of future population change to show that population growth will have a large impact on heat stress in the region. We also find that humidity change will make extreme heat worse than if there was only increase in air temperature. Our results show the importance of using smaller grid sizes to provide information about future heat stress that might be more relevant for people living in these regions than can be found from global models.

## 1. Introduction

The Great Lakes Region (GLR) is the largest megalopolis in the world, home to almost 100 million people, and an ecologically important area of both the United States and Canada (Lang & Knox, 2009; Wuebbles et al., 2019). It also plays a critical role in both country's economies, with major industries such as manufacturing, agriculture, and tourism (Krantzberg & De Boer, 2008; Bhavsar et al., 2010). The region is facing several challenges due to climate change, including the threat of future extreme heat (Byun & Hamlet, 2018; Wuebbles et al., 2019). As global temperatures continue to rise, the region is expected to experience more heat wave days (Lopez et al., 2018). These heat waves can have serious consequences for human health, as they can lead to heat stroke, dehydration, and other heat-related illnesses (Ebi et al., 2021). They can also have negative impacts on the environment, such as through increased droughts and wildfire (Kerr et al., 2018; Brown et al., 2021; Gamelin et al., 2022).

In addition to direct health and environmental risks, extreme heat can have indirect negative impacts. Extreme heat can harm the region's agriculture industry by reducing crop yields and by harming livestock (Tubiello et al., 2007; Jin et al., 2017). It can also affect tourism, as high heat stress can make outdoor activities unpleasant and can lead to the closure of beaches and other attractions (Matthews et al., 2021). Additionally, warming can put a strain on the region's energy infrastructure, as increased air conditioning use can lead to higher demand for electricity (Obringer et al., 2022; Tan et al., 2022).

To address these challenges and become resilient to future warming, it is important to develop strategies for mitigating and adapting to future heat stress. This involves both improving heat warning systems and emergency response plans, as well as implementing measures to reduce heat-related health risks. It could also involve investing in technologies and infrastructure that can help to reduce the impact of extreme heat. Planning relevant mitigation and adaptation strategies require accurate estimates of future extreme heat. However, projections of extreme heat from Earth System Model (ESMs) are frequently too coarse to appropriately resolve regional warming signals (Pierce et al., 2009; Lloyd et al., 2021). For instance, populations in the GLR are concentrated around the Great Lakes, but the coarse resolution at which ESMs are run cannot isolate climate change at those relevant scales (Byun & Hamlet, 2018).

While statistical downscaling is often used to get regional warming signals from coarse ESM outputs (Hayhoe et al., 2010; Byun & Hamlet, 2018), these methods presuppose an unchanged distribution of the underlying data under different climate conditions (Spak et al., 2007; Dixon et al., 2016; Lanzante et al., 2018), which is not useful for examining discontinuous climatology, as often seen near water bodies, or for dealing with weather extremes. Additionally, most future projections focus on air temperature, even though heat stress depends on multiple additional factors, including humidity, wind speed, and radiation (Anderson et al., 2013; Heo et al., 2019). To address these gaps, we use a pseudo global warming (PGW) approach to estimate the range of end-of-the-century extreme heat stress over the GLR for the shared socio-economic pathway 5 (SSP5), which is the worst-case scenario equivalent to fossil fueled Representative Concentration Pathways (RCP) 8.5 scenario (Riahi et al., 2011). Our PGW approach uses data from 11 Coupled Model Intercomparison Project phase 6 (CMIP6) ESMs to provide future projected changes to the initial and boundary conditions (derived from reanalysis data) to the Weather Research and Forecasting (WRF) model, which can be run at spatiotemporal scales relevant for isolating regional climate change. We then combine these dynamically downscaled model outputs with corresponding population projections to examine population-level heat stress exposure over this region. The manuscript is divided into three main sections, with section 2 describing the methods, section 3 presenting the main results, and section 4 discussing some of the implications and limitations of the study.

## 2. Methods

### 2.1 Pseudo global warming simulations over the Great Lakes Region

The WRF model (version 4.2.2) with the Advanced Research WRF dynamic core (Skamarock & Klemp, 2008) is used for both historical and future scenarios at a spatial resolution of 4 km (J. Wang et al., 2022). For the historical scenario, WRF uses initial and boundary conditions derived from the 3-hourly 0.25° European Centre for Medium-Range Weather Forecasts atmospheric reanalysis of the global climate, version 5 (ERA5; Hersbach et al., 2020). The lake surface temperature (LST) is derived from the National Oceanic and Atmospheric Administration's GLSEA satellite estimates (Schwab et al., 1999), which is at a spatial resolution of 1.3 km and has been previously found to be a better source for the lake boundary conditions than ERA5 (J. Wang et al., 2022). The WRF model incorporates Thompson microphysics (Thompson et al., 2004, 2008), the Rapid Radiative Transfer Model for GCMs longwave and shortwave schemes (Iacono et al., 2008), and the Unified Noah land surface model by Chen and Dudhia (2001). Multi-layer urban canopy model with building energy and building environment parameterizations (Martilli et al., 2002; Salamanca et al., 2010) are coupled with Noah and the Mellor–Yamada–Janjić scheme (Janjić, 1994) is used to simulate the planetary boundary layer. While incorporating the urban canopy model increases computational costs, this physics configuration has been found to better capture air temperature, skin temperature, and wind speed diurnal cycles compared to experiments using Noah LSM alone (J. Wang et al., 2023).

For the future scenario, we use a PGW approach (Kimura, 2007) to estimate near end-of-the-century climate over GLR for the SSP5 scenario. We use 11 ESMs from CMIP6 (see Table 1) to provide future projected changes in near surface and upper-level variables that are needed to drive the WRF simulations. These variables include 3-dimensional air temperature, specific humidity, geopotential height, as well as surface pressure, sea-level pressure, and skin temperature. The changes are calculated between past (1981-2010) and the future (2071-2100) periods using monthly CMIP6 datasets. These changes are then added to the corresponding 3 hourly values from ERA5 to generate new boundary conditions for WRF for the future scenario. The new lower boundary conditions for lakes (that is the LST) is obtained by adding the changes in skin temperature from ESMs to the GLSEA satellite derived LST. Perturbations to wind patterns are not explicitly considered from the ESM data as they are calculated by WRF based on the thermodynamic changes due to the new boundary conditions of temperature, pressure, and specific humidity. While the lakes may not be accurately represented in ESMs (with different parameterizations in different ESMs), their subgrid changes in ESMs are the only available data source. Moreover, we mainly focus on the changes over land in the present study. All ESMs show increases in air temperature and specific humidity, with E3SM (Exascale Earth System Model; Golaz et al., 2019) being the warmest and FGOALS (Flexible Global Ocean-Atmosphere-Land System; Zhou et al., 2014) being the coolest when looking at the GLR regional temperature changes.

In addition to running the WRF with each individual ESM, an ensemble mean (ENS) is generated by averaging the WRF outputs from the 11 simulations. We show results from WRF driven by the ENS, E3SM and FGOALS to demonstrate a range of possibilities for the future scenarios. Our main region of interest for most of the analysis is the bounding box around the Great Lakes Basin (Fig. 1a), which we refer to as the GLR. Our model domain extends beyond this region. The smaller region of interest compared to the entire model domain helps minimize the boundary issues at the domain edges.

Table 1. Overview of ESMs used to run PGW simulations in the present study.

| ESM name | Spatial resolution | Reference |
|---|---|---|
| **ACCESS-CM2** | 1.25x1.88 | Bi et al., 2020 |
| **CanESM5** | 2.79x2.81 | Swart et al., 2019 |
| **FGOALS-f3-L** | 2.79 x 2.81 | Zhou et al., 2014 |
| **MIROC6** | 1.40x1.41 | Tatebe et al., 2019 |
| **CESM-WACCM** | 1.88 x 2.5 | Marsh et al., 2013 |
| **E3SM-1-1** | 1 x 1 | Golaz et al., 2019 |
| **GFDL-CM4** | 2.00 x 2.50 | Held et al., 2019 |
| **MPI-ESM1-2-LR** | 1.86 x 1.88 | Jungclaus et al., 2013 |
| **CMCC-CM2-SR5** | 0.75x 0.75 | Cherchi et al., 2019 |
| **EC-Earth3** | 1.12x1.13 | Döscher et al., 2022 |
| **IPSL-CM6A-LR** | 1.89x3.75 | Boucher et al., 2020 |
| **NorESM2-LM** | 1.89x2.5 | Seland et al., 2020 |

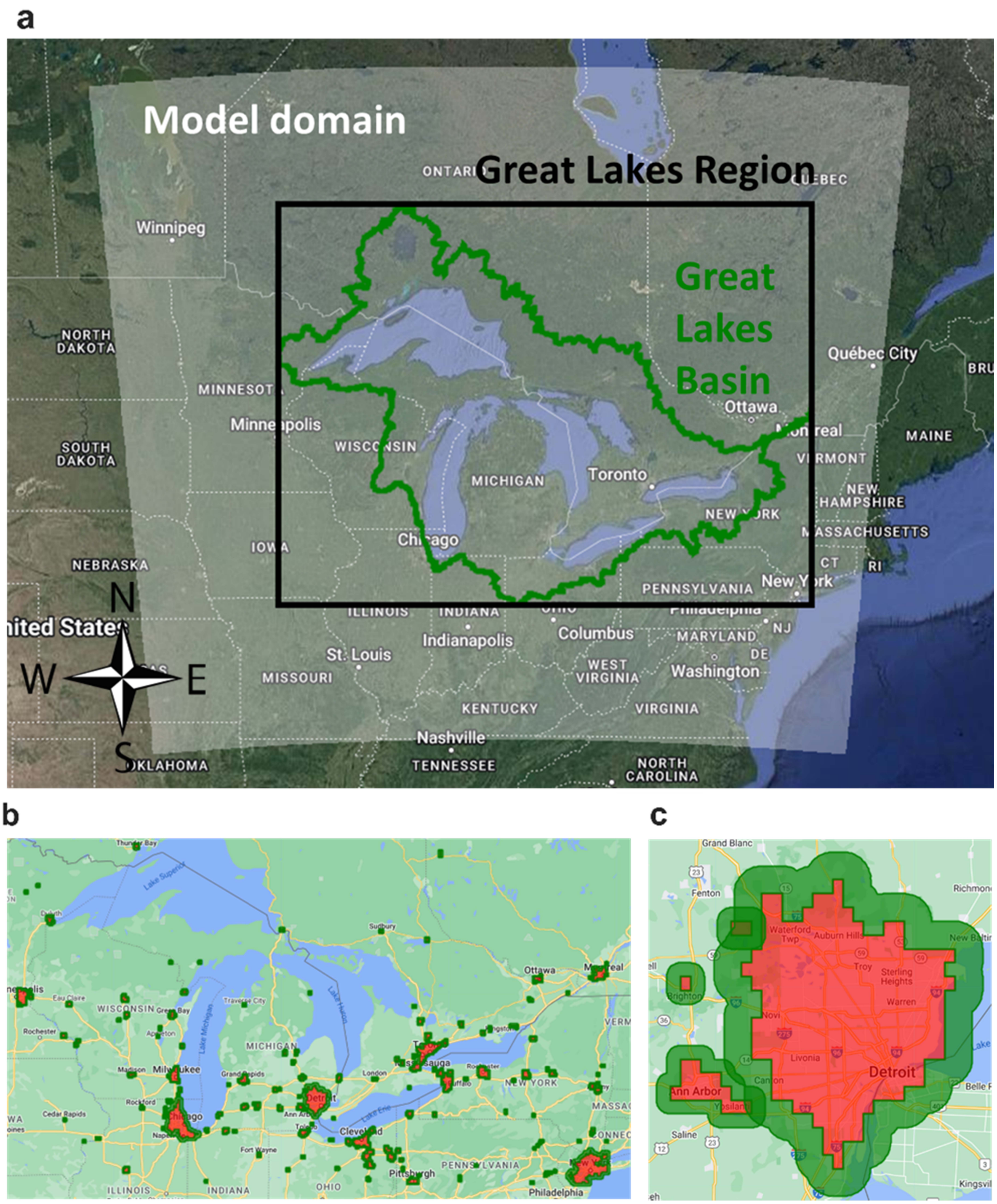


**Figure 1.** Multiple regions of interest used in the present study. Sub-figure (a) shows the model domain, the Great Lakes Basin, as well as the bounding box around the basin representing the Great Lakes Region. Sub-figure (b) shows all urban clusters (in red) within the region, as well as their normalized rural buffers (in green). Sub-figure (c) shows an

example of a few urban clusters surrounding and including Detroit and their corresponding normalized buffers. Basemap Source: Google

## 2.2 Calculating heat stress indices and their sensitivities to input factors

The human physiological response to heat depends on multiple factors, including air temperature and relative humidity (Anderson et al., 2013; Chakraborty et al., 2022). To estimate human-relevant heat stress exposure, here we consider two metrics of heat stress – namely heat index and the wet bulb globe temperature. The heat index, also known as apparent temperature, considers both temperature and moisture content of the air, with the later impacting the body's ability to dissipate heat through sweating. This index is calculated in multiple steps (Rothfusz, 1990). First, a simple formula (Eq. 1) is applied to calculate an initial heat index value consistent with the results from Steadman (1979).

$$\mathrm{HI} = 0.5 \times [\mathrm{AT} + 61 + [(\mathrm{AT}-68) \times 1.2] + (0.094\mathrm{RH})] \tag{1}$$

where AT is in °F and RH is in percentage. If the average of this value and the air temperature is less than 80°F, this initial value is used as the final heat index. If the average is equal to or above 80°F, a more complex formula (Eq. 2), called the Rothfusz regression, is used instead.

$$\begin{aligned}\mathrm{HI} \quad &= -42.379 + 2.04901523 \times \mathrm{AT} + 10.14333127 \times \mathrm{RH} - 0.22475541 \times \mathrm{AT} \times \mathrm{RH} - 6.83783 \\ &\times 10^{-3} \times \mathrm{AT}^2 - 5.481717 \times 10^{-2} \times \mathrm{RH}^2 + 1.22874 \times 10^{-3} \times \mathrm{AT}^2 \times \mathrm{RH} + 8.5282 \\ &\times 10^{-4} \times \mathrm{AT} \times \mathrm{RH}^2 - 1.99 \times 10^{-6} \times \mathrm{AT}^2 \times \mathrm{RH}^2\end{aligned} \tag{2}$$

Additional adjustments are made for low and high values of humidity. The heat index is used by the U.S. National Weather Service (NWS) in operational heat warning systems.

Wet bulb globe temperature is the second heat index we use to measure heat stress. It is a weighted average of air temperature, natural wet-bulb temperature, and black globe temperature. The black globe temperature considers radiant heat, air temperature, and wind speed, making this a more comprehensive index that considers the effects of radiation and wind on heat stress (Heo et al., 2019). In this study, wet bulb globe temperature is calculated using Eq. 3, where SR and WS are solar insolation (in kW $m^{-2}$) and wind speed (in m $s^{-1}$), respectively, and AT is in °C.

$$\mathrm{WBGT} = 0.735 \times \mathrm{AT} + 0.0374 \times \mathrm{RH} + 0.00292 \times \mathrm{AT} \times \mathrm{RH} + 7.619 \times \mathrm{SR} - 4.557 \times \mathrm{SR}^2 - 0.0572 \times \mathrm{WS} - 4.064 \tag{3}$$

The heat indices are calculated for both the historical and future scenarios. In addition to calculating these indices using all input variables from each scenario, we examine sensitivities of the indices to their input factors through a perturbation analysis. This is done by keeping all factors but one the same as the historical values and changing one of them to its future values. Since air temperature and relative humidity are strongly correlated, to disentangle these interactions, when we isolate the impact of temperature change on future heat stress, we keep the specific humidity (not relative humidity) the same as the historical case. Taking the heat indiex as an example, the difference between the overall change (both temperature and relative humidity are from future scenarios) and the change due to only the increase in air temperature represents the humidity feedback.

### 2.3 Estimating future population-adjusted heat stress extremes over land

While heat stress extremes are important, the regional impacts of extreme heat would depend on the covariance of these extremes with populations. At coarse ESM resolutions, regional hotspots cannot be resolved, which is why we need these high spatial and temporal resolution regional climate simulations. We first subset our simulations to only consider values over land, where the majority of the population lives. Then, we combine (grid-wise multiplication, see below) our WRF simulations with downscaled 1 km population projections (Jones et al., 2020) for the SSP5 scenario. For historical scenarios, the SSP5 population projections for the year 2020 are used, to represent present conditions, and for the future simulations, the average of the projections for 2070, 2080, 2090, and 2100 to match the years used to generate the future projected changes in the PGW approach. Although the WRF simulations are for the year 2018, the Jones et al. (2020) dataset is only available every 10 years, and here we attempt to use the same population dataset for consistency. Finally, we examine grid-wise population, heat stress above critical thresholds, and population-adjusted heat extremes (person-hours) by multiplying the WRF outputs with the spatially corresponding population estimates. All the geospatial analysis of the model outputs are done on the Google Earth Engine platform (Gorelick et al., 2017).

### 2.4 Separating the urban signal from the background climate

Urban areas are important hotspots of human-relevant heat impacts since they have higher populations than nearby rural areas as well as local-scale warming (urban heat island effect;

Qian et al., 2022). To estimate this urban signal, we first generate urban clusters based on groups of contiguous urban grids, as used in the WRF surface dataset (Fig. 1b). For each cluster, a normalized buffer area is defined such that this buffered area is approximately equal to the area of the cluster it is associated with. We use an iterative method implemented on Google Earth Engine (Gorelick et al., 2017) using a step size of 4 km to create these buffers. Similar methods have often been used to determine the surface urban heat island intensity using satellite observations (Chakraborty et al., 2021). Urban heat index and wet bulb globe temperature islands are calculated for the GLR as the difference in the heat stress metrics over land between the urban clusters and their buffered areas. Since urban clusters may sometimes be within the buffer of another nearby cluster (see Fig. 1c), all urban grids are masked out from the rural reference before calculating the background heat stress values.

## 3. Results

### 3.1 Heat stress extremes in the present and future

We first examine the distributions of hourly domain-averaged air temperature, heat index, and wet bulb globe temperature over the entire model domain to provide baselines from these simulations (Fig. 2). The mean summer air temperature increases from 19.2 °C in HIST to 29.2 °C in E3SM. The ensemble mean domain-averaged air temperature at the end of the century is 25.9 °C (Fig. 2a). Similarly, the domain-averaged heat index increases from 19.4 °C in HIST to 33.3 °C in E3SM. The U.S. NWS places heat risk into four main categories based on heat index, namely “Caution” (>=80 °F and <90 °F or >=26.7 °C and <32.2 °C), “Extreme Caution” (>=90 °F and <103 °F or >=32.2 °C and <39.4 °C), “Danger” (>=103 °F and <125 °F or >=39.4 °C and <51.7 °C), and “Extreme Danger” (>=51.7 °F).  Although there are slight regional differences in these thresholds, we choose the most common thresholds over the US. Based on the model simulations, the mean domain-average heat index will cross into the “Danger” territory in E3SM and into the “Extreme Caution” territory from ENS (Fig. 2b). Similarly, wet bulb globe temperature can be categorized into “Low” (>=80 °F and <85 °F or >=26.7 °C and <29.4 °C), “Moderate” (>=85 °F and <88 °F or >=29.4 °C and <31.1 °C), “High” (>=88 °F and <90 °F or >=31.1 °C and <32.2 °C), and “Extreme” (>=90 °F or >=32..2 °C) (Mullin, 2022). Although wet bulb globe temperature has not been an operational metric from the NWS, that changed in June of 2022. The mean wet bulb globe temperature increases from 18.2 °C in HIST to 26.3 °C for E3SM (23.9 °C for ENS). Although domain-averaged value does not cross into any of the critical thresholds, even for E3SM, a large fraction of the summer hours fall into them (Fig. 2c). For instance, although none of the summer hours in HIST are in “High” or above category, around 12% of the hours are for E3SM by the end-of-century (~0.3% for ENS).

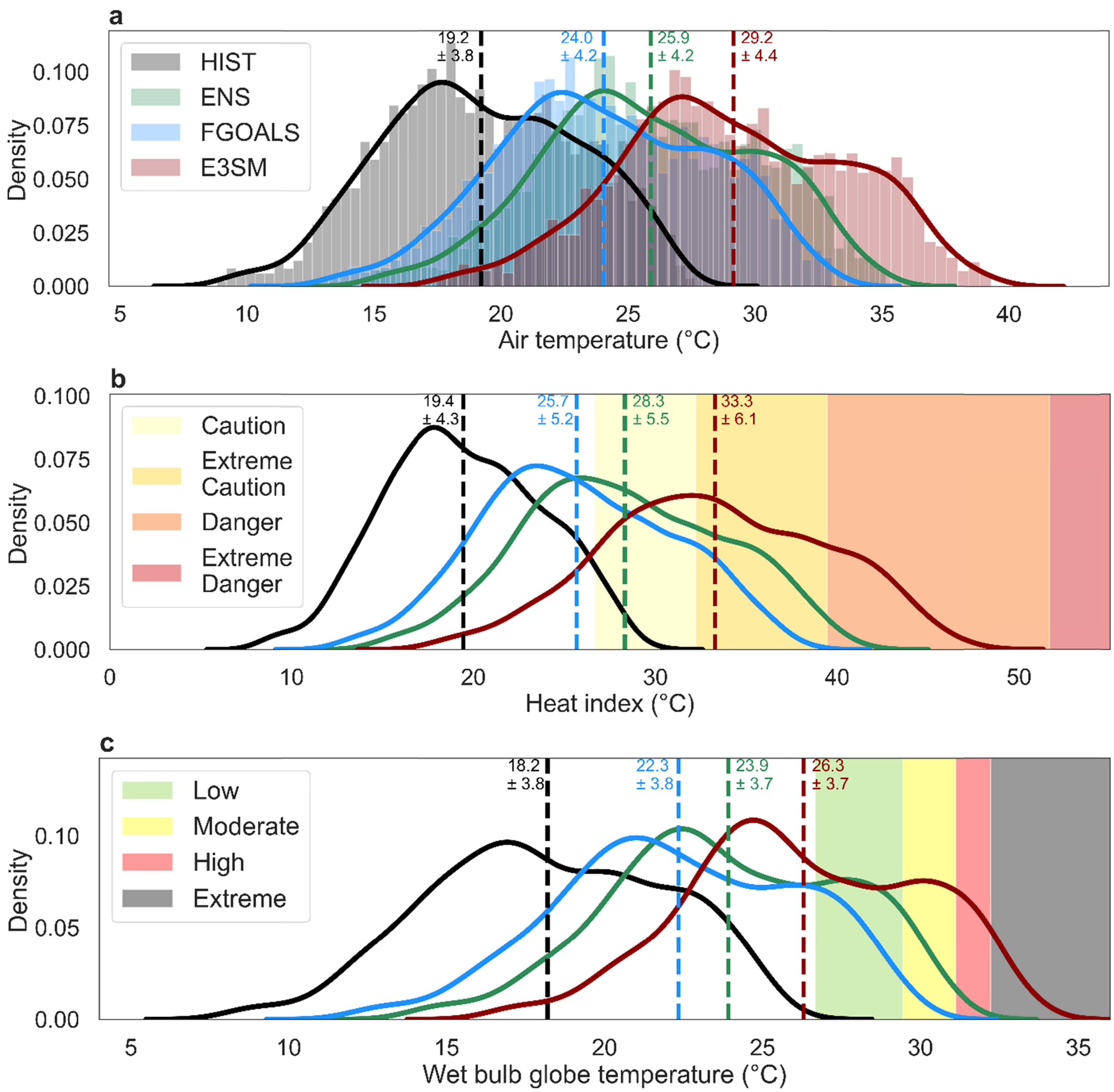


**Figure 2.** Summertime distribution of domain-averaged hourly (a) air temperature, (b) heat index, and (c) wet bulb globe temperature from the model simulations. The mean and standard deviation are noted for each simulation. For heat index and wet bulb globe temperature, the

U.S. National Weather Service thresholds for heat risk categories considered in the present study are shown.

When we separate the hourly data into daytime and nighttime based on the presence and absence, respectively, of incoming solar radiation, we expectedly see higher values during daytime (Fig. 3). The mean daytime heat index touches the “Caution” territory even in the coolest model (FGOALS; Fig. 3c). Similarly, mean wet bulb globe temperature from E3SM touches the “Low” territory during daytime (Fig. 3e). For both daytime air temperature and heat index, the spreads in hourly domain-averaged values are higher in the future compared to the HIST simulation. This (higher standard deviation for future heat stress and air temperature) is also seen for all summer hourly distributions (Figs 2a, 2b). On the other hand, for wet bulb globe temperature, the spread remains either largely unchanged or reduced in the future projections compared to the historical scenario. This is probably because, unlike heat index, WBGT also depends on wind speed and solar radiation, which are negative feedbacks on future wet bulb globe temperature (see Section 3.4).

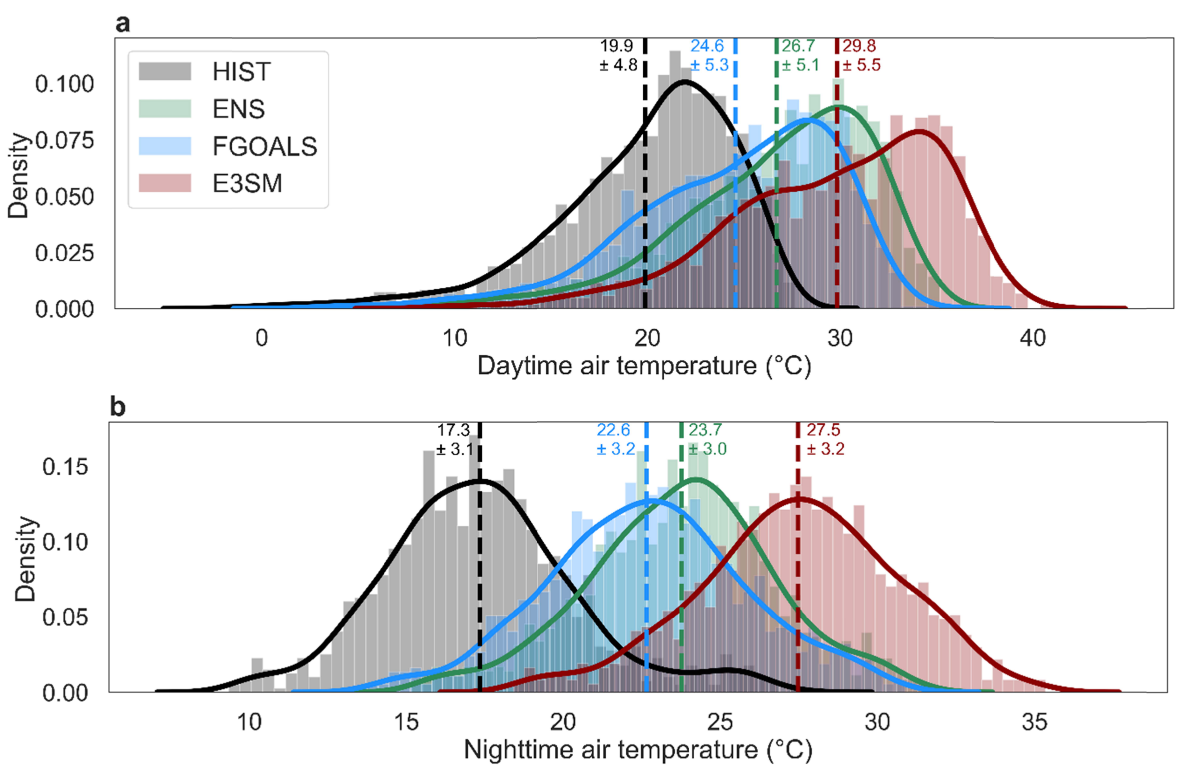

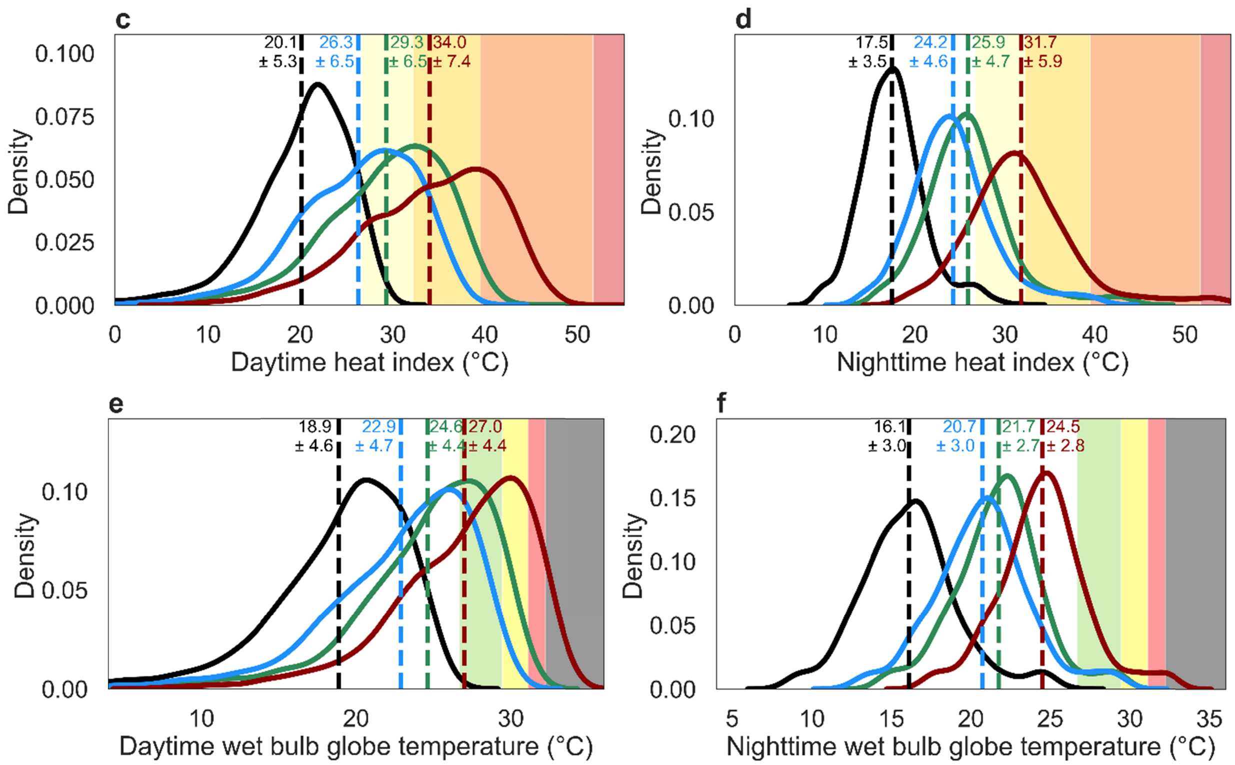


**Figure 3.** Summertime distribution of domain-averaged hourly (a) daytime air temperature, (b) nighttime air temperature, (c) daytime heat index, (d) nighttime heat index, (e) daytime wet bulb globe temperature and (f) nighttime wet bulb globe temperature from the model simulations. The mean and standard deviation are noted for each simulation. For heat index and wet bulb globe temperature, the U.S. National Weather Service thresholds for heat risk categories considered in the present study (see Fig. 2) are shown.

## 3.2 Summertime heat stress exceedance over land

Since there is large spatial variability in climate over land, looking at domain-averaged values does not provide a full picture of hotspots of heat stress extremes. So, we examine grid-wise percentage hourly exceedance of the heat stress indices for a typical summer, this time focusing on the land grids within GLR. Results are shown for the “Danger” category for heat index (Fig. 4) and the “High” category for wet-bulb globe temperature (Fig. 5). In the HIST simulation, the percentage of summer hours in the “Danger” category and above varies between 0 and 2%, with larger values generally in the southwest of the region. In the future, the percentage of hours rises significantly, varying from 0 to 30% for FGOALS, 0 to 45% for ENS, and 0 to 80% for E3SM. Therefore, even if the FGOALS projections, representing the lower bound for SSP5, materialize, parts of the GLR would have heat indices in the “Danger” category for close to 30% of the summer (and over half of the daytime hours). Some of these hotspots are clearly seen, including over Chicago along the south-west shore of Lake Michigan (Figs 4b 4c, 4d). Sudden changes in exceedances are also seen along the shores of most of the lakes, which represents the coastal interactions that impact both temperature and humidity (J. Wang et al., 2023).

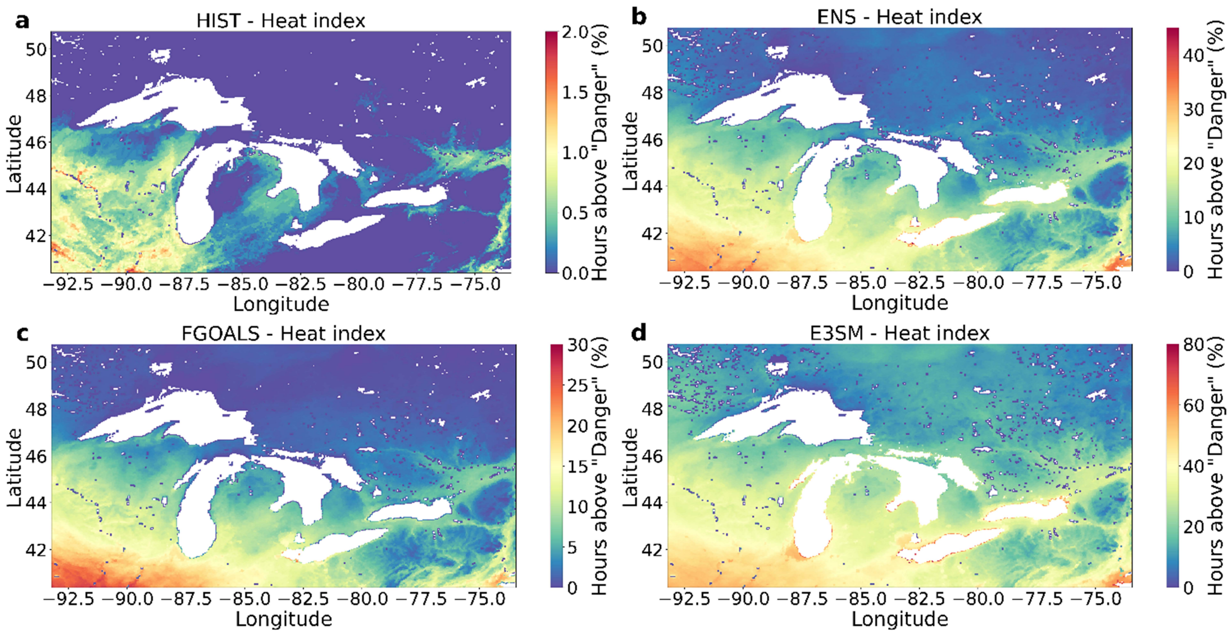


**Figure 4.** Spatial distribution of percentage of hours with heat index above the “Danger” heat risk category for (a) HIST, (b) ENS, (c) FGOALS, and (d) E3SM simulations for a typical summer.

Similarly, for wet bulb globe temperature, the percentage of hours above the “High” category in a typical summer is between 0 and 1.4% in HIST (Fig. 5). The upper bound will rise to 25% for FGOALS, 30% for ENS, and 60% for E3SM. Overall, in the SSP5 scenario, future summer heat would pose a significant heat risk for outdoor activities regardless of the model used. Like Fig. 4, sharp gradients are seen along the shores of the Great Lakes and even the Atlantic coastline visible in the southeast of GLR. In other words, along the Great Lakes coasts, the lake breeze and other effects are dampening some of the heat risk.

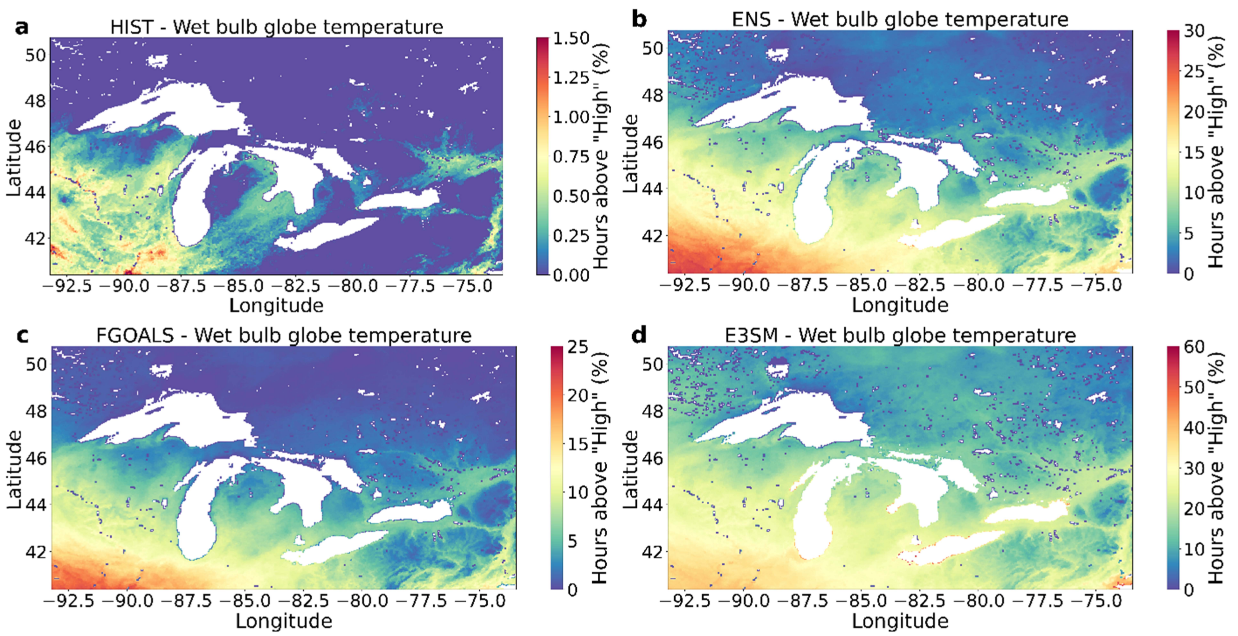


**Figure 5.** Spatial distribution of percentage of hours with wet bulb globe temperature above the "High" heat risk category for (a) HIST, (b) ENS, (c) FGOALS, and (d) E3SM simulations for a typical summer.

## 3.3 Present and future population-adjusted heat exposure

To get an estimate of human impacts of extreme heat, we should focus on where people live (Tuholske et al., 2021). In addition to global warming, populations are projected to change significantly over GLR under the SSP5 scenario (Pendall et al., 2017). The population-adjusted heat risk, which we define here as the number of people in a grid multiplied by the number of summer hours above critical heat stress thresholds, will rise substantially. For instance, for heat index, the maximum person-hours above "Danger" category will be over an order of magnitude higher than HIST for the ENS case (Figs 6a, 6b).

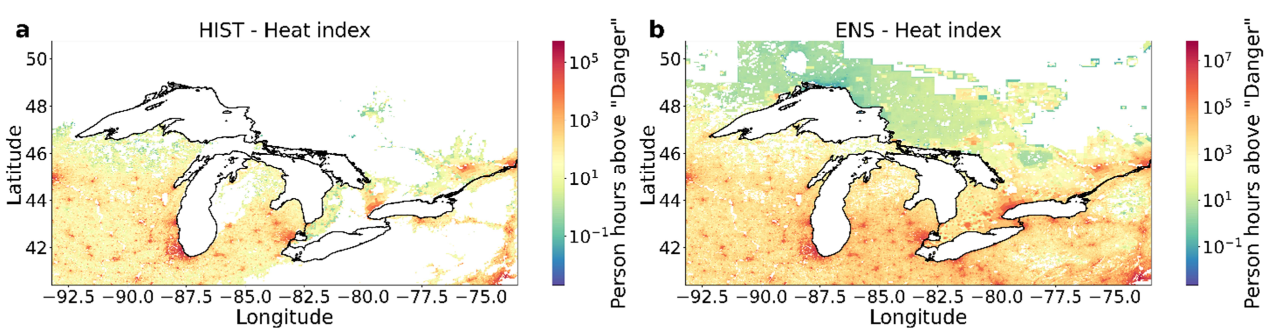

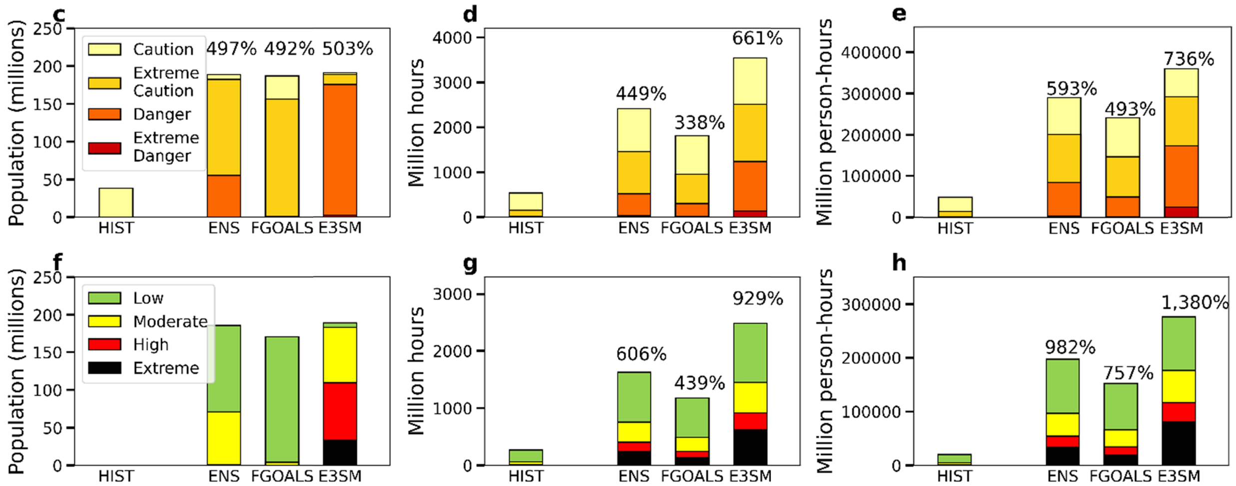


**Figure 6.** Population-adjusted heat stress over the Great Lakes Region. Sub-figs (a) and (b) show person-hours above the "Danger" category for heat index for HIST and ENS, respectively. The white grids have zero person-hours above the "Danger" category. Sub-fig (c) shows overall population living in grids with heat index in "Caution" and above category for more than 25% of summer, while (d) shows the number of cumulative million hours in each category in the region for all simulations. Sub-fig (e) shows the million person-hours in each category for all simulations. Sub-figs (f), (g), and (h) are similar to (c), (d), and (e), but for wet bulb globe temperature. Percentage changes from the baseline are shown when baselines are non-zero.

We calculate the total population in GLR who, currently or in the future, will live in regions where the heat index lies in the "Caution" and above territory for 25% or more of the hours in summer. This amounts to around 38 million for HIST and over 185 million (191.08 million for E3SM, 188.59 million for ENS, and 186.87 million for FGOALS) for all the future scenarios. Throughout the GLR, the number of hours above the "Caution" and above category increases from 536 million in HIST to over 3544 million over E3SM. Similar increases are seen for million hours above "Low" category for wet bulb globe temperature, with increases of around 929% for E3SM for the baseline HIST simulation (606% for ENS). One goal of this analysis is to examine population-level exposure to heat extremes and the role of population growth on overall heat exposure in the region. To do this, we can compare the percentage change in million person-hours of heat stress above thresholds to the percentage change in only heat extremes without accounting for population. In all cases (Figs 6d, 6e, 6g, and 6h), the change in cumulative population-adjusted heat exposure is higher than the cumulative heat exposure. For heat index, population growth increases person-hours of heat index above “Caution” category by 11.3% for E3SM, 31.9% for ENS, and 45.9% for FGOALS. Results for all scenarios and heat risk categories are compiled in Table 2.

Table 2: Summary of percentage increases in person-hours above heat stress categories during summer at the end of the century due to population growth in the Great Lakes Region.

| | Percentage increase in person-hour exposure due to population growth (%) | | | | | | |
|---|---|---|---|---|---|---|---|
| | Heat Index above | | | Wet bulb globe temperature above | | | |
| Scenario | Caution | Extreme Caution | Danger | Low | Moderate | High | Extreme |
| ENS | 31.9 | 43.4 | 121.4 | 62.1 | 69.3 | 78 | 89.4 |
| FGOALS | 45.9 | 60.2 | 123.2 | 72.4 | 78.6 | 91 | 95.3 |
| E3SM | 11.3 | 21.1 | 90.1 | 48.6 | 61.3 | 68.9 | 79.2 |

Here we only consider one estimate of future population, which is combined with all model simulations. Therefore, since the change in person-hours is a function of both the population growth and the ESM-simulated warming, the population contribution is always lower for the warmer models (Table 2). Additionally, in all cases, the population growth contribution is larger for higher heat stress categories. This would mathematically make sense if regions that have higher heat stress have higher population growth in the future. In the GLR, higher populations are generally seen in the southern parts, where it is much warmer, while populations are low or close to zero in the northern parts, mainly in Canada. In the future, while populations will shift to some of these northern regions according to the population projections (Fig. 6b), relative population growth will still be higher in the warmer subregions.

An important pattern for examining population-adjusted heat stress is this spatial covariance between population and mean summer heat indices. In all scenarios and for both heat index and wet bulb globe temperature, more populated regions within GLR tend to have higher mean heat stress (Fig. 7). This is seen from positive correlations between the two, even though the variability in heat stress is not associated with the variability in population. In the future, the sensitivity of heat index to unit change in population will decrease according to all the models.

This suggests that population growth will tend to be higher in regions that have lower heat stress within the GLR. This is seen for both heat index and wet bulb globe temperature. Overall, regions within GLR with disproportionately stronger heat stress coincide with regions with higher population in the present and this association is projected to become weaker in the future.

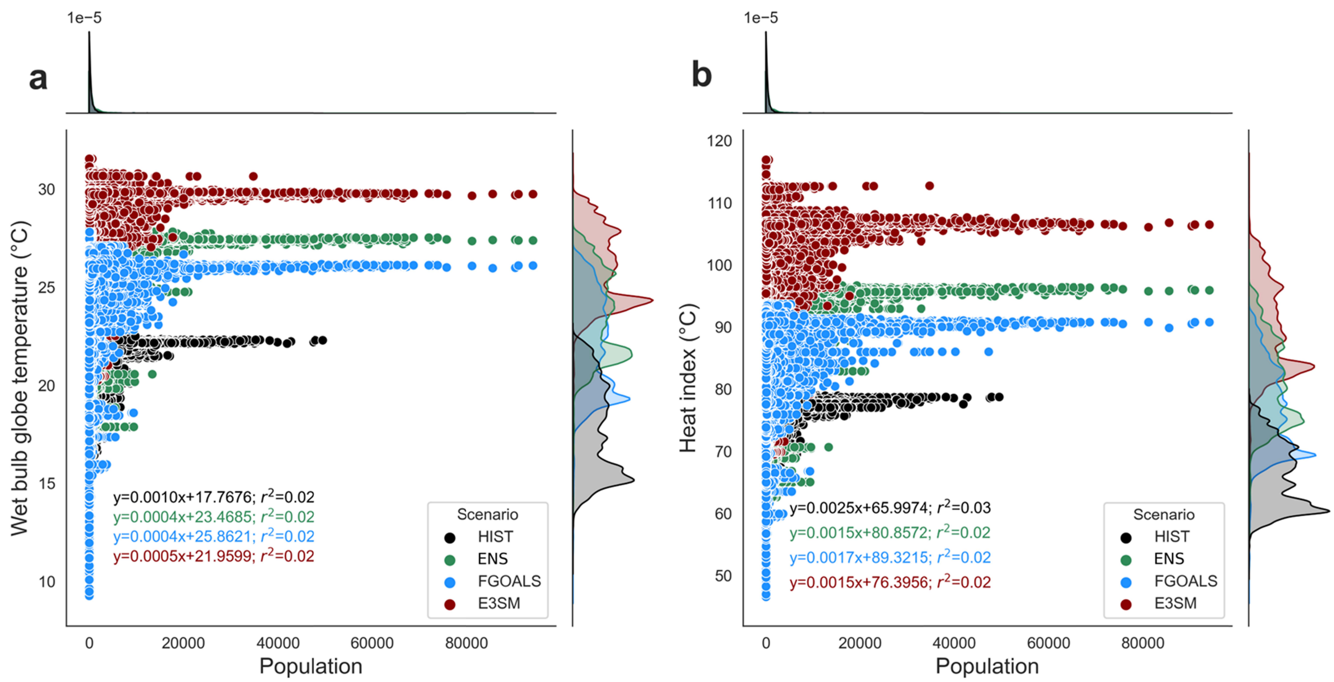


**Figure 7.** Distributions of population and heat indices over the Great Lakes Region. Plots show grid-wise associations between population and mean summer (a) heat index and (b) wet bulb globe temperature (against baseline population for HIST and against future population projections for ENS, FGOALS, and E3SM). The distributions of the variables are shown on the right and top (for baseline population) panels. Equations for lines of best fit between the population and the heat indices, along with the coefficients of determination, are also noted.

## 3.4 Factor contributions to future heat stress

There has been increased discussion about humid heat, its changes in the past, and projected increases in the future due to its greater relevance to human health (Sherwood & Huber, 2010; Willett & Sherwood, 2012; Coffel et al., 2017; Pal & Eltahir, 2016; Raymond et al., 2020; Mishra et al., 2020). Since increases in air temperature also influences moisture capacity, and the GLR region has several local and regional moisture sources, it is important to understand the relative contributions of air temperature and relative humidity on future humid heat stress. We find that, in all cases, the actual increase in heat stress is higher than what it would have been had only the air temperature changed. Or, in other words, humidity change is a positive feedback that amplifies future heat stress over GLR. This makes conceptual sense since an increase in air temperature without a change in moisture amount (absolute vapor pressure) would reduce relative humidity by increasing the saturation vapor pressure. However, in reality, the absolute vapor pressure also increases in a wetter future (W. Wang et al., 2021), meaning relative humidity will be higher than expected from changes in air temperature alone. It is this relative humidity that modulates overall cooling ability though sweating, and thus the physiological response to extreme heat ( Sherwood & Huber, 2010; Anderson et al., 2013; Ioannou et al., 2022). However, the increase in air temperature still explains most of the increase in mean heat stress over GLR (Fig. 8), ranging from 55.7% for wet bulb globe temperature for FGOALS to over 80.5% for heat index for FGOALS. Regionally, more variations are seen, though the contributions from air temperature still dominate (Fig. 8c). Of note, the contributions from air temperature are consistently found to be higher for heat index than for wet bulb globe temperature, which is because heat index is a strong function of air temperature (Chakraborty et al., 2022; Sherwood, 2018).

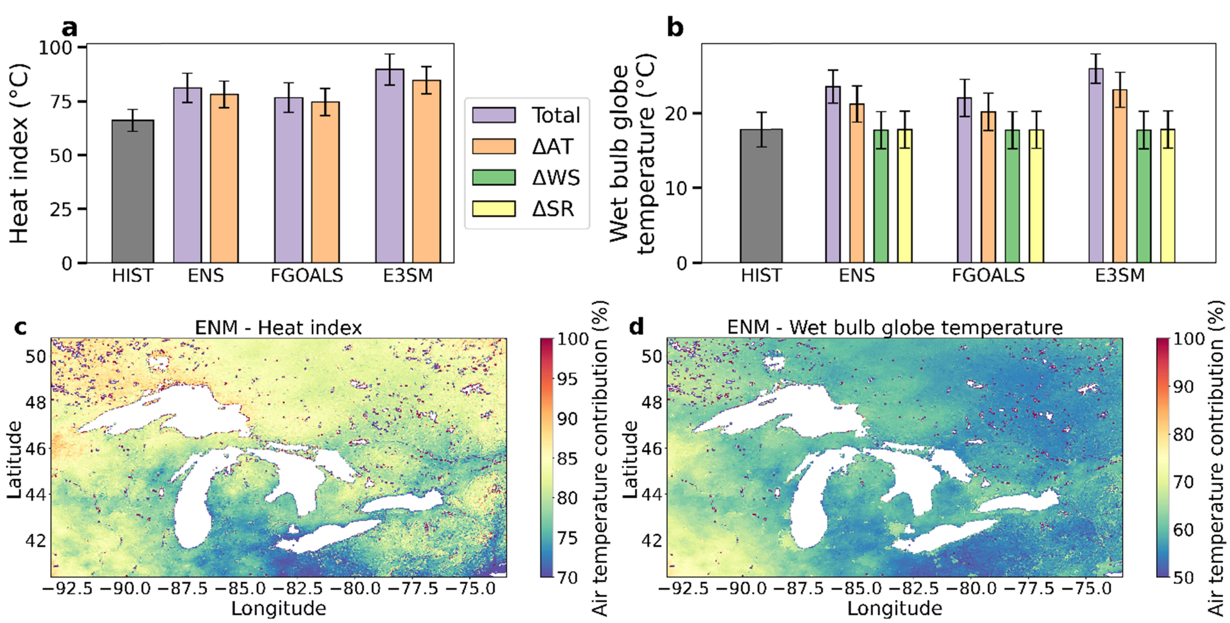


**Figure 8.** Contribution of factors to future heat stress. The bars show historical (a) heat index and (b) wet bulb globe temperature, and corresponding future values for different scenarios,

once by changing all factors to their future estimates, and again by only changing individual factors to their future estimates and keeping historical values of other factors. The error bars represent the stand deviation across space for each case. Sub-figures (c) and (d) show grid-wise contribution of temperature to overall change in summer heat index and wet bulb globe temperature, respectively, in the future for the ENS scenario.

The positive humidity feedback amplifying future heat stress is also seen when separating the model results into daytime and nighttime. The air temperature contribution generally stays between 50 and 80% of the overall change in heat stress metrics, with the humidity feedback dominating slightly (temperature contribution ~49.6%) for nighttime wet bulb globe temperature in FGOALS. For wet bulb globe temperature, we also examine the impact of the change in wind speed and solar radiation (assuming these changes are independent of changes in air temperature and specific humidity) and find their contributions to be minor in comparison to air temperature and humidity. The contribution maxes out at -3.7% due to wind speed change on daytime wet bulb globe temperature increase in FGOALS. Contributions from both wind speed and solar radiation are negative, as in the changes in wind speed and solar radiation in the future tends to reduce heat stress in all cases.

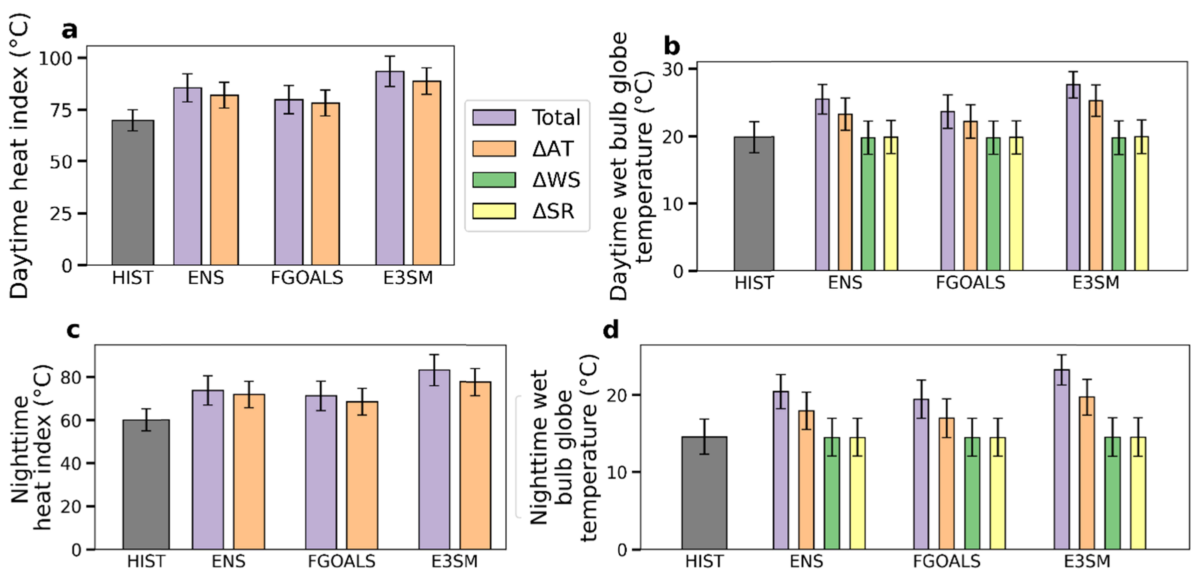


**Figure 9.** Contribution of factors to future heat stress during day and night. The bars show historical (a) daytime heat index and (b) daytime wet bulb globe temperature, and corresponding future values for different scenarios, once by changing all factors to their future

estimates, and again by only changing individual factors to their future estimates and keeping historical values of other factors. The error bars represent the stand deviation across space for each case. Sub-figures (c) and (d) are same as (a) and (b), but for nighttime.

3.5 Present and future urban heat stress signal

Urban areas are notable hotspots of heat risk due to higher population and heat islands. We separate the heat stress into their urban and rural components and estimate heat stress islands equivalent to commonly studied urban heat islands (Qian et al., 2022). We see larger nighttime urban heat stress island compared to daytime values, which is consistent with both observational and modeling estimates (Sarangi et al., 2021; Chakraborty et al., 2022).This diurnality is retained in the future, with all models showing higher nighttime values for both urban heat index and wet bulb globe temperature islands (Fig. 10). Changes in the urban heat stress islands are minor, but with interesting distinctions. Daytime urban heat index island generally decreases in the future while the nighttime values increase slightly, which is consistent with the results in Sarangi et al. (2021). However, urban daytime wet bulb globe temperature island increases during daytime and decreases during nighttime. This is potentially related to the role of the other factors that are considered in wet bulb globe temperature and the different sensitivity of this index to humidity. Note that there are several simplifications in urban representation in these models that would strongly impact these results (see Discussion).

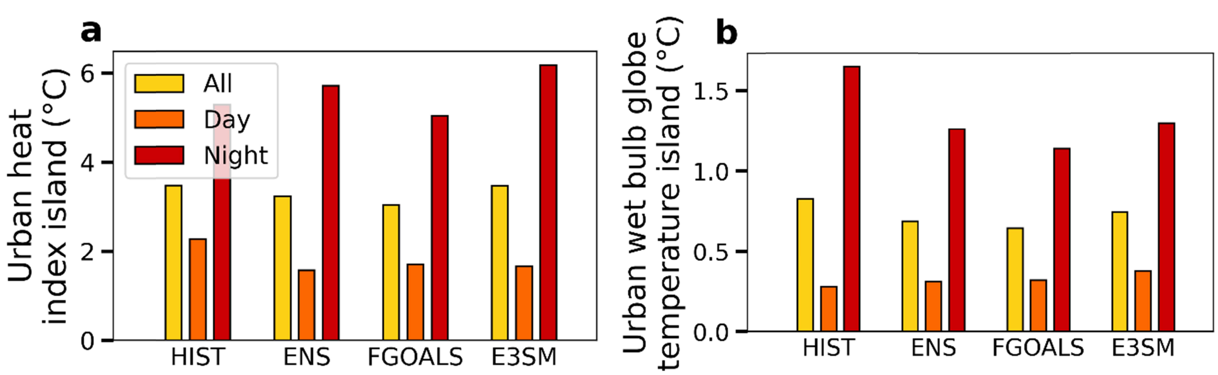


**Figure 10.** Urban heat stress signals in the present and future. The bar plots show overall, daytime, and nighttime heat stress islands in the Great Lakes Region for different scenarios using (a) heat index and (b) wet bulb globe temperature, respectively.

## 4. Discussion

A large majority of studies on future warming have focused on air temperature (Pörtner et al., 2022), which ignores the impact of humidity and other factors on heat stress and how these physical changes covary with demographic shifts. Additionally, many projections of future heat stress use statistical downscaling techniques that cannot resolve real climate signals beyond their assumed statistical distributions (Byun & Hamlet, 2018; Jang & Kavvas, 2015). Using PGW simulations based on multiple ESM projections, we dynamically downscale future climate projections, isolate the role of humidity on future summertime heat stress, and examine spatial covariance between the heat hazard and population over GLR. Overall, major increases in heat stress are projected under SSP5 in GLR towards the end of the century, with a large percentage of summer hours exceeding critical heat risk thresholds defined by the U.S. NWS. The role of humidity on overall heat stress is also substantial and can account for up to half the future increase in heat stress, with regional variations. Of note, we find that the two heat stress metrics currently used by the NWS have largely different sensitivities to humidity, which can impact the magnitude of heat risk in future climate assessments. It is however important to stress that the separation of the contribution of humidity from air temperature is only done considering the direct effects. We assume that, while the water holding capacity increases with temperature due to thermodynamic constraints, the specific humidity would not change as a direct consequence of warming. However, higher temperatures can indirectly increase specific humidity by modifying the surface energy budget, particularly evapotranspiration, and strengthening the hydrological cycle. These impacts are harder to isolate quantitatively, have multiple competing effects, and are strongly dependent on model parameterizations. As such, our contribution estimates likely represent the upper bound for humidity and the lower bound for air temperature.

The combined impact of high temperatures and humidity can have significant public health consequences, particularly for vulnerable populations such as the elderly and those with pre-existing health conditions (Mora et al., 2017). Positive associations are seen between heat stress and population, suggesting disproportionate heat impacts when accounting for population-level risks. This population growth will likely bring both opportunities and challenges to the region, including the need for increased infrastructure, housing, and public services. It is important for policy makers and decision makers to consider the potential impacts of population growth and take steps to manage and sustainably develop the region. For instance, population growth and rising temperatures are both expected to increase the demand for air conditioning (Obringer et al., 2022), which can further exacerbate heat stress events if increased energy demands are not met. This lack of access to air conditioning was a mortality factor during the 1999 Chicago heat wave (Naughton et al., 2002). Although urban areas do not show significant changes in the local urban heat stress signal in the future, they still support large population densities, leading to disproportionate impacts at the population scale. As such, urban adaptation strategies, such as increasing access to cooling centers and improving urban planning, will be important for optimizing adaptation to future heat stress events in GLR.

It is important to discuss uncertainties in the present study that should be considered when contextualizing these results. These uncertainties rise from, among other things, the scenarios chosen, the model biases, and the population projections. Here we only focus on the RCP8.5 scenario, even though it has become less likely based on present pathways (Pielke Jr et al., 2022). This is designed as a worst-case estimate, and we do not expect the core results and insights to change for relatively cooler scenarios other than in terms of the numbers. Model biases are potentially the biggest source of uncertainty. Since ESMs show large variability in future climate estimates across models, we choose 11 ESMs to provide a range of possibilities instead of a single estimate. There are similarly large uncertainties in WRF that rise from representation of land cover, lakes, cloud parameterizations, and the model configuration chosen (Sharma et al., 2014; Qian et al., 2022; J. Wang et al., 2022), though these uncertainties are expected to be smaller in magnitude than the differences across ESMs. For instance, no transient land cover change is considered here, which may influence surface climate, though it is expected to be less important than the changes in atmospheric forcing in the future. Moreover, since projected urban expansion is not accounted for in these WRF simulations (Gao & O’Neill, 2020), we may be underestimating the urban heat stress islands. While the urban signal was a minor component of the present analysis, future urban heat stress estimates should consider urban growth. Finally, the population projections are somewhat dated and statistically downscaled, which may overestimate future population growth and insufficiently resolve local-scale demographic distributions.

## Conclusions

Uncertainties in regional-scale future climate change projections are prevalent, with coarse-grained ESMs not resolving spatial variabilities sufficiently. This study uses pseudo global warming simulations at spatiotemporal resolutions relevant for human heat exposure based on 11 state-of-the-art ESMs to examine changes in summer heat stress extremes in the GLR using both heat index and wet bulb globe temperature. Combining these downscaled climate projections with future population estimates reveals the population versus warming contributions to heat stress in the GLR, with population growth almost doubling population-weighted outdoor heat stress exposure in the region. Our results show that significant parts of summer will experience critical outdoor heat stress in the GLR. Humidity change amplifies heat stress compared to changing air temperature alone, with the humidity control depending on the heat stress metric used. On the other hand, wind speed and shortwave radiation, which are required to compute wet bulb globe temperature are negative feedbacks for future heat stress. Overall, this study provides a range of future heat stress estimates based on multiple ESMs for the upper end SSP5 scenario and highlights the importance of dynamically resolving heat stress at population-relevant scales for more accurate regional heat risk assessments.

## References


Anderson, G. B., Bell, M. L., & Peng, R. D. (2013). Methods to Calculate the Heat Index as an Exposure Metric in Environmental Health Research. *Environmental Health Perspectives*, *121*(10), 1111–1119. https://doi.org/10.1289/ehp.1206273

Bhavsar, S. P., Gewurtz, S. B., McGoldrick, D. J., Keir, M. J., & Backus, S. M. (2010). Changes in mercury levels in Great Lakes fish between 1970s and 2007. *Environmental Science & Technology*, *44*(9), 3273–3279.

Bi, D., Dix, M., Marsland, S., O'farrell, S., Sullivan, A., Bodman, R., Law, R., Harman, I., Srbinovsky, J., & Rashid, H. A. (2020). Configuration and spin-up of ACCESS-CM2, the new generation Australian community climate and earth system simulator coupled model. *Journal of Southern Hemisphere Earth Systems Science*, *70*(1), 225–251.

Boucher, O., Servonnat, J., Albright, A. L., Aumont, O., Balkanski, Y., Bastrikov, V., Bekki, S., Bonnet, R., Bony, S., & Bopp, L. (2020). Presentation and evaluation of the IPSL-CM6A-LR climate model. *Journal of Advances in Modeling Earth Systems*, *12*(7), e2019MS002010.

Brown, E. K., Wang, J., & Feng, Y. (2021). US wildfire potential: A historical view and future projection using high-resolution climate data. *Environmental Research Letters*, *16*(3), 034060.

Byun, K., & Hamlet, A. F. (2018). Projected changes in future climate over the Midwest and Great Lakes region using downscaled CMIP5 ensembles. *International Journal of Climatology*, *38*, e531–e553.

Chakraborty, T., Sarangi, C., & Lee, X. (2021). Reduction in human activity can enhance the urban heat island: Insights from the COVID-19 lockdown. *Environmental Research Letters*.

Chakraborty, T., Venter, Z., Qian, Y., & Lee, X. (2022). *Lower urban humidity moderates heat stress* [Preprint]. Meteorology. https://doi.org/10.1002/essoar.10511293.1

Chen, F., & Dudhia, J. (2001). Coupling an advanced land surface–hydrology model with the Penn State–NCAR MM5 modeling system. Part I: Model implementation and sensitivity. *Monthly Weather Review*, *129*(4), 569–585.

Cherchi, A., Fogli, P. G., Lovato, T., Peano, D., Iovino, D., Gualdi, S., Masina, S., Scoccimarro, E., Materia, S., & Bellucci, A. (2019). Global mean climate and main patterns of variability in the CMCC-CM2 coupled model. *Journal of Advances in Modeling Earth Systems*, *11*(1), 185–209.

Coffel, E. D., Horton, R. M., & De Sherbinin, A. (2017). Temperature and humidity based projections of a rapid rise in global heat stress exposure during the 21st century. *Environmental Research Letters*, *13*(1), 014001.

Dixon, K. W., Lanzante, J. R., Nath, M. J., Hayhoe, K., Stoner, A., Radhakrishnan, A., Balaji, V., & Gaitán, C. F. (2016). Evaluating the stationarity assumption in statistically downscaled climate projections: Is past performance an indicator of future results? *Climatic Change*, *135*(3), 395–408.

Döscher, R., Acosta, M., Alessandri, A., Anthoni, P., Arsouze, T., Bergman, T., Bernardello, R., Boussetta, S., Caron, L.-P., & Carver, G. (2022). The EC-Earth3 earth system model for the coupled model intercomparison project 6. *Geoscientific Model Development*, *15*(7), 2973–3020.

Ebi, K. L., Capon, A., Berry, P., Broderick, C., de Dear, R., Havenith, G., Honda, Y., Kovats, R. S., Ma, W., & Malik, A. (2021). Hot weather and heat extremes: Health risks. *The Lancet*, *398*(10301), 698–708.

Gamelin, B. L., Feinstein, J., Wang, J., Bessac, J., Yan, E., & Kotamarthi, V. R. (2022). Projected US drought extremes through the twenty-first century with vapor pressure deficit. *Scientific Reports*, *12*(1), 1–15.

Gao, J., & O'Neill, B. C. (2020). Mapping global urban land for the 21st century with data-driven simulations and Shared Socioeconomic Pathways. *Nature Communications*, *11*(1), 1–12.

Golaz, J.-C., Caldwell, P. M., Van Roekel, L. P., Petersen, M. R., Tang, Q., Wolfe, J. D., Abeshu, G., Anantharaj, V., Asay-Davis, X. S., & Bader, D. C. (2019). The DOE E3SM coupled model version 1: Overview and evaluation at standard resolution. *Journal of Advances in Modeling Earth Systems*, *11*(7), 2089–2129.

Gorelick, N., Hancher, M., Dixon, M., Ilyushchenko, S., Thau, D., & Moore, R. (2017). Google Earth Engine: Planetary-scale geospatial analysis for everyone. *Remote Sensing of Environment*, *202*, 18–27. https://doi.org/10.1016/j.rse.2017.06.031

Hayhoe, K., VanDorn, J., Croley II, T., Schlegal, N., & Wuebbles, D. (2010). Regional climate change projections for Chicago and the US Great Lakes. *Journal of Great Lakes Research*, *36*, 7–21.

Held, I. M., Guo, H., Adcroft, A., Dunne, J. P., Horowitz, L. W., Krasting, J., Shevliakova, E., Winton, M., Zhao, M., & Bushuk, M. (2019). Structure and performance of GFDL's CM4. 0 climate model. *Journal of Advances in Modeling Earth Systems*, *11*(11), 3691–3727.

Heo, S., Bell, M. L., & Lee, J.-T. (2019). Comparison of health risks by heat wave definition: Applicability of wet-bulb globe temperature for heat wave criteria. *Environmental Research*, *168*, 158–170.

Hersbach, H., Bell, B., Berrisford, P., Hirahara, S., Horányi, A., Muñoz-Sabater, J., Nicolas, J., Peubey, C., Radu, R., & Schepers, D. (2020). The ERA5 global reanalysis. *Quarterly Journal of the Royal Meteorological Society*, *146*(730), 1999–2049.

Iacono, M. J., Delamere, J. S., Mlawer, E. J., Shephard, M. W., Clough, S. A., & Collins, W. D. (2008). Radiative forcing by long-lived greenhouse gases: Calculations with the AER radiative transfer models. *Journal of Geophysical Research: Atmospheres*, *113*(D13).

Ioannou, L. G., Tsoutsoubi, L., Mantzios, K., Vliora, M., Nintou, E., Piil, J. F., Notley, S. R., Dinas, P. C., Gourzoulidis, G. A., & Havenith, G. (2022). Indicators to assess physiological heat strain–Part 3: Multi-country field evaluation and consensus recommendations. *Temperature*, 1–18.

Jang, S., & Kavvas, M. L. (2015). Downscaling global climate simulations to regional scales: Statistical downscaling versus dynamical downscaling. *Journal of Hydrologic Engineering*, *20*(1), A4014006.

Janjić, Z. I. (1994). The step-mountain eta coordinate model: Further developments of the convection, viscous sublayer, and turbulence closure schemes. *Monthly Weather Review*, *122*(5), 927–945.

Jin, Z., Zhuang, Q., Wang, J., Archontoulis, S. V., Zobel, Z., & Kotamarthi, V. R. (2017). The combined and separate impacts of climate extremes on the current and future US rainfed maize and soybean production under elevated CO2. *Global Change Biology*, *23*(7), 2687–2704.

Jones, B., O'Neill, B. C., & Gao, J. (2020). *Global 1-km Downscaled Population Base Year and Projection Grids for the Shared Socioeconomic Pathways (SSPs), Revision 01* [Data set]. Palisades, NY: NASA Socioeconomic Data and Applications Center (SEDAC). https://doi.org/10.7927/Q7Z9-9R69

Jungclaus, J. H., Fischer, N., Haak, H., Lohmann, K., Marotzke, J., Matei, D., Mikolajewicz, U., Notz, D., & Von Storch, J. S. (2013). Characteristics of the ocean simulations in the Max Planck Institute Ocean Model (MPIOM) the ocean component of the MPI-Earth system model. *Journal of Advances in Modeling Earth Systems*, *5*(2), 422–446.

Kerr, G. H., DeGaetano, A. T., Stoof, C. R., & Ward, D. (2018). Climate change effects on wildland fire risk in the Northeastern and Great Lakes states predicted by a downscaled multi-model ensemble. *Theoretical and Applied Climatology*, *131*(1), 625–639.

Kimura, F. (2007). Downscaling by pseudo global warming method. The Final Report of the ICCAP. Research Institute for Humanity and Nature (RIHN), Kyoto, Japan. *Undefined*. https://www.semanticscholar.org/paper/Downscaling-by-pseudo-global-warming-method.-The-of-Kimura/a9743bb92b237a9368ecdf3f3df7a20fd2f5cf10

Krantzberg, G., & De Boer, C. (2008). A valuation of ecological services in the Laurentian Great Lakes Basin with an emphasis on Canada. *Journal-American Water Works Association*, *100*(6), 100–111.

Lang, R., & Knox, P. K. (2009). The new metropolis: Rethinking megalopolis. *Regional Studies*, *43*(6), 789–802.

Lanzante, J. R., Dixon, K. W., Nath, M. J., Whitlock, C. E., & Adams-Smith, D. (2018). Some pitfalls in statistical downscaling of future climate. *Bulletin of the American Meteorological Society*, *99*(4), 791–803.

Lloyd, E. A., Bukovsky, M., & Mearns, L. O. (2021). An analysis of the disagreement about added value by regional climate models. *Synthese*, *198*(12), 11645–11672.

Lopez, H., West, R., Dong, S., Goni, G., Kirtman, B., Lee, S.-K., & Atlas, R. (2018). Early emergence of anthropogenically forced heat waves in the western United States and Great Lakes. *Nature Climate Change*, *8*(5), 414–420.

Marsh, D. R., Mills, M. J., Kinnison, D. E., Lamarque, J.-F., Calvo, N., & Polvani, L. M. (2013). Climate change from 1850 to 2005 simulated in CESM1 (WACCM). *Journal of Climate*, *26*(19), 7372–7391.

Martilli, A., Clappier, A., & Rotach, M. W. (2002). An urban surface exchange parameterisation for mesoscale models. *Boundary-Layer Meteorology*, *104*(2), 261–304.

Matthews, L., Scott, D., & Andrey, J. (2021). Development of a data-driven weather index for beach parks tourism. *International Journal of Biometeorology*, *65*(5), 749–762.

Mishra, V., Ambika, A. K., Asoka, A., Aadhar, S., Buzan, J., Kumar, R., & Huber, M. (2020). Moist heat stress extremes in India enhanced by irrigation. *Nature Geoscience*, *13*(11), 722–728. https://doi.org/10.1038/s41561-020-00650-8

Mora, C., Dousset, B., Caldwell, I. R., Powell, F. E., Geronimo, R. C., Bielecki, C. R., Counsell, C. W. W., Dietrich, B. S., Johnston, E. T., Louis, L. V., Lucas, M. P., McKenzie, M. M., Shea, A. G., Tseng, H., Giambelluca, T. W., Leon, L. R., Hawkins, E., & Trauernicht, C. (2017). Global risk of deadly heat. *Nature Climate Change*, *7*(7), 501–506. https://doi.org/10.1038/nclimate3322

Mullin, S. (2022). *An Analysis of Wet Bulb Globe Temperature Estimation Methods and Microclimate Heat Variability in Columbia, South Carolina*.

Naughton, M. P., Henderson, A., Mirabelli, M. C., Kaiser, R., Wilhelm, J. L., Kieszak, S. M., Rubin, C. H., & McGeehin, M. A. (2002). Heat-related mortality during a 1999 heat wave in Chicago. *American Journal of Preventive Medicine*, *22*(4), 221–227.

Obringer, R., Nateghi, R., Maia-Silva, D., Mukherjee, S., Cr, V., McRoberts, D. B., & Kumar, R. (2022). Implications of increasing household air conditioning use across the United States under a warming climate. *Earth's Future*, *10*(1), e2021EF002434.

Pal, J. S., & Eltahir, E. A. B. (2016). Future temperature in southwest Asia projected to exceed a threshold for human adaptability. *Nature Climate Change*, *6*(2), 197–200. https://doi.org/10.1038/nclimate2833

Pendall, R., Poethig, E., Treskon, M., Blumenthal, E., & Center, U. I. M. H. and C. P. (2017). *The future of the great lakes region*. Urban Institute, Metropolitan Housing and Communities Policy Center.

Pielke Jr, R., Burgess, M. G., & Ritchie, J. (2022). Plausible 2005–2050 emissions scenarios project between 2° C and 3° C of warming by 2100. *Environmental Research Letters*, *17*(2), 024027.

Pierce, D. W., Barnett, T. P., Santer, B. D., & Gleckler, P. J. (2009). Selecting global climate models for regional climate change studies. *Proceedings of the National Academy of Sciences*, *106*(21), 8441–8446.

Pörtner, H.-O., Roberts, D. C., Adams, H., Adler, C., Aldunce, P., Ali, E., Begum, R. A., Betts, R., Kerr, R. B., & Biesbroek, R. (2022). Climate change 2022: Impacts, adaptation and vulnerability. *IPCC Sixth Assessment Report*.

Qian, Y., Chakraborty, T. C., Li, J., Li, D., He, C., Sarangi, C., Chen, F., Yang, X., & Leung, L. R. (2022). Urbanization Impact on Regional Climate and Extreme Weather: Current Understanding, Uncertainties, and Future Research Directions. *Advances in Atmospheric Sciences*. https://doi.org/10.1007/s00376-021-1371-9

Raymond, C., Matthews, T., & Horton, R. M. (2020). The emergence of heat and humidity too severe for human tolerance. *Science Advances*, *6*(19), eaaw1838. https://doi.org/10.1126/sciadv.aaw1838

Riahi, K., Rao, S., Krey, V., Cho, C., Chirkov, V., Fischer, G., Kindermann, G., Nakicenovic, N., & Rafaj, P. (2011). RCP 8.5—A scenario of comparatively high greenhouse gas emissions. *Climatic Change*, *109*(1), 33–57.

Rothfusz, L. P., & Headquarters, N. S. R. (1990). The heat index equation (or, more than you ever wanted to know about heat index). *Fort Worth, Texas: National Oceanic and Atmospheric Administration, National Weather Service, Office of Meteorology*, *9023*.

Salamanca, F., Krpo, A., Martilli, A., & Clappier, A. (2010). A new building energy model coupled with an urban canopy parameterization for urban climate simulations—Part I. formulation, verification, and sensitivity analysis of the model. *Theoretical and Applied Climatology*, *99*(3), 331–344.

Sarangi, C., Qian, Y., Li, J., Ruby Leung, L., Chakraborty, T. C., & Liu, Y. (2021). Urbanization amplifies nighttime heat stress on warmer days over the US. *Geophysical Research Letters*, e2021GL095678.

Schwab, D. J., Leshkevich, G. A., & Muhr, G. C. (1999). Automated mapping of surface water temperature in the Great Lakes. *Journal of Great Lakes Research*, *25*(3), 468–481.

Seland, Ø., Bentsen, M., Olivié, D., Toniazzo, T., Gjermundsen, A., Graff, L. S., Debernard, J. B., Gupta, A. K., He, Y.-C., & Kirkevåg, A. (2020). Overview of the Norwegian Earth System Model (NorESM2) and key climate response of CMIP6 DECK, historical, and scenario simulations. *Geoscientific Model Development*, *13*(12), 6165–6200.

Sharma, A., Fernando, H. J. S., Hellmann, J., & Chen, F. (2014). Sensitivity of WRF Model to Urban Parameterizations, With Applications to Chicago Metropolitan Urban Heat Island. *Volume 1D, Symposia: Transport Phenomena in Mixing; Turbulent Flows; Urban Fluid Mechanics; Fluid Dynamic Behavior of Complex Particles; Analysis of Elementary Processes in Dispersed Multiphase Flows; Multiphase Flow With Heat/Mass Transfer in Process Technology; Fluid Mechanics of Aircraft and Rocket Emissions and Their Environmental Impacts; High Performance CFD Computation; Performance of Multiphase Flow Systems; Wind Energy; Uncertainty Quantification in Flow Measurements and Simulations*, V01DT28A002. https://doi.org/10.1115/FEDSM2014-21292

Sherwood, S. C. (2018). How Important Is Humidity in Heat Stress? *Journal of Geophysical Research: Atmospheres*, *123*(21). https://doi.org/10.1029/2018JD028969

Sherwood, S. C., & Huber, M. (2010). An adaptability limit to climate change due to heat stress. *Proceedings of the National Academy of Sciences*, *107*(21), 9552–9555. https://doi.org/10.1073/pnas.0913352107

Skamarock, W. C., & Klemp, J. B. (2008). A time-split nonhydrostatic atmospheric model for weather research and forecasting applications. *Journal of Computational Physics*, *227*(7), 3465–3485.

Spak, S., Holloway, T., Lynn, B., & Goldberg, R. (2007). A comparison of statistical and dynamical downscaling for surface temperature in North America. *Journal of Geophysical Research: Atmospheres*, *112*(D8).

Steadman, R. G. (1979). The assessment of sultriness. Part I: A temperature-humidity index based on human physiology and clothing science. *Journal of Applied Meteorology and Climatology*, *18*(7), 861–873.

Swart, N. C., Cole, J. N., Kharin, V. V., Lazare, M., Scinocca, J. F., Gillett, N. P., Anstey, J., Arora, V., Christian, J. R., & Hanna, S. (2019). The Canadian earth system model version 5 (CanESM5. 0.3). *Geoscientific Model Development*, *12*(11), 4823–4873.

Tan, H., Kotamarthi, R., Wang, J., Qian, Y., & Chakraborty, T. C. (2022). Impact of different roofing mitigation strategies on near-surface temperature and energy consumption over the Chicago metropolitan area during a heatwave event. *Science of The Total Environment*, 160508.

Tatebe, H., Ogura, T., Nitta, T., Komuro, Y., Ogochi, K., Takemura, T., Sudo, K., Sekiguchi, M., Abe, M., & Saito, F. (2019). Description and basic evaluation of simulated mean state, internal variability, and climate sensitivity in MIROC6. *Geoscientific Model Development*, *12*(7), 2727–2765.

Thompson, G., Field, P. R., Rasmussen, R. M., & Hall, W. D. (2008). Explicit forecasts of winter precipitation using an improved bulk microphysics scheme. Part II: Implementation of a new snow parameterization. *Monthly Weather Review*, *136*(12), 5095–5115.

Thompson, G., Rasmussen, R. M., & Manning, K. (2004). Explicit forecasts of winter precipitation using an improved bulk microphysics scheme. Part I: Description and sensitivity analysis. *Monthly Weather Review*, *132*(2), 519–542.

Tubiello, F. N., Soussana, J.-F., & Howden, S. M. (2007). Crop and pasture response to climate change. *Proceedings of the National Academy of Sciences*, *104*(50), 19686–19690.

Tuholske, C., Caylor, K., Funk, C., Verdin, A., Sweeney, S., Grace, K., Peterson, P., & Evans, T. (2021). Global urban population exposure to extreme heat. *Proceedings of the National Academy of Sciences*, *118*(41).

Wang, J., Qian, Y., Pringle, W., Chakraborty, T. C., Hetland, R., Yang, Z., & Xue, P. (2023). Contrasting effects of lake breeze and urbanization on heat stress in Chicago metropolitan area. *Urban Climate*, *48*, 101429. https://doi.org/10.1016/j.uclim.2023.101429

Wang, J., Xue, P., Pringle, W., Yang, Z., & Qian, Y. (2022). Impacts of Lake Surface Temperature on the Summer Climate Over the Great Lakes Region. *Journal of Geophysical Research: Atmospheres*, *127*(11). https://doi.org/10.1029/2021JD036231

Wang, W., Chakraborty, T. C., Xiao, W., & Lee, X. (2021). Ocean surface energy balance allows a constraint on the sensitivity of precipitation to global warming. *Nature Communications*, *12*(1), 2115. https://doi.org/10.1038/s41467-021-22406-7

Willett, K. M., & Sherwood, S. (2012). Exceedance of heat index thresholds for 15 regions under a warming climate using the wet-bulb globe temperature. *International Journal of Climatology*, *32*(2), 161–177.

Wuebbles, D., Cardinale, B., Cherkauer, K., Davidson-Arnott, R., Hellmann, J., Infante, D., Johnson, L., de Loë, R., Lofgren, B., & Packman, A. (2019). An assessment of the impacts of climate change on the Great Lakes. *Environmental Law & Policy Center*.

Zhou, T., Yu, Y., Liu, Y., & Wang, B. (2014). *Flexible global ocean-atmosphere-land system model: A modeling tool for the climate change research community*. Springer.

## Acknowledgments

This study is supported by COMPASS-GLM, a multi-institutional project supported by the U.S. Department of Energy, Office of Science, Office of Biological and Environmental Research as part of the Regional and Global Modeling and Analysis (RGMA) program, Multi-sector Dynamics Modeling (MSD) program, and Earth System Model Development (ESMD) program. This study is also Contribution No. 92 of the Great Lakes Research Center at Michigan Technological University. Computational resources are provided by the DOE-supported National Energy Research Scientific Computing Center and Argonne Leadership Computing Facility. The Pacific Northwest National Laboratory is operated for DOE by Battelle Memorial Institute under contract DE-AC05-76RL01830.

## Author contributions

T.C. conducted the analysis and wrote the manuscript. Z.Y. processed the ESM data. Both Z.Y. and J.W. ran the WRF simulations and J.W. calculated the heat stress indices. All co-authors contributed to research design, writing, and revision.

## Open Research

The WRF model code is open source and can be accessed at: https://github.com/wrf-model/WRF. All regional summaries and rasters presented in the present study can be found on Zenodo: https://doi.org/10.5281/zenodo.7603277

## Competing interests

The authors declare no competing financial or non-financial interests.